

Electronic Supplementary Information

Iron-Based Thin Films as Highly Efficient Catalysts for Electrochemical Water Oxidation in Carbonate Electrolyte

Fei Li,^{a,†,*} Lichen Bai,^{a,†} Hua Li^a, Yong Wang^a, Fengshou Yu^a, and Licheng Sun^{a,b}

a. State Key Laboratory of Fine Chemicals, DUT-KTH Joint Education and Research Center on Molecular Devices, Dalian University of Technology (DUT), 116024 Dalian, China. E-mail: lifei@dlut.edu.cn

b. Department of Chemistry, School of Chemical Science and Engineering, KTH Royal Institute of Technology, 10044 Stockholm, Sweden.

† These authors contribute equally to this work.

General materials and instruments

Ultra pure water ($18.2 \text{ M}\Omega\text{cm}^{-1}$) for all the reactions or measurements was obtained from a Milli-Q system (Millipore, Direct-Q 3 UV). $\text{FeSO}_4 \cdot 7\text{H}_2\text{O}$ (99.95%), NaHCO_3 (99.5%), Na_2CO_3 (99.99%) and NaOH (99.0%) was purchased from Aladdin Industrial Corporation. High purity Ar (99.999%) and CO_2 (99.999%) were acquired from Dalian Guangming Co., Ltd. Other chemical reagents were analytical pure and used without further purification. Fluorine-doped tin oxide (FTO) substrates were purchased from Dalian Heptachroma SolarTech Co., Ltd. (thickness of $\sim 2.2 \text{ mm}$, transmittance of $>90\%$, resistance of $\sim 15 \text{ }\Omega/\text{cm}^2$).

SEM images and EDX spectra were obtained by using a Nova NanoSEM 450 equipment. Images were obtained with an acceleration voltage of 3 kV and EDX

spectra were obtained with acceleration voltage of 20 kV. The content of the catalyst was quantified by an Inductively Coupled Plasma-Atomic Emission (ICP-AES) spectrometer (Optima 2000DV, America PerkinElmer Corp.) TEM images were obtained by using a FEI TF30 equipment. The sample used for this was prepared by modification the Fe-Ci film on FTO of 12 cm² (3 cm × 4 cm) through 500s electrodeposition with applied bias as 1.37 V vs. NHE. The resulting electrode was rinsed gently with de-ionized water and dried in air, and then carefully scraped off using a doctor blade. The combined material was dispersed in absolute ethanol by ultrasound, and a drop of the mixture was dried on a carbon-coated copper grid for analysis. PXRD was collected by a D/max-2400 diffractometer (Japan Rigaku Rotaflex) using Cu K α radiation ($\lambda = 154.1$ nm). X-ray photoelectron spectroscopy (XPS) measurement was performed on a Thermo Scientific ESCALAB250 instrument using 200 W K α radiation. The binding energy (BE) was calibrated with respect to the C 1s level 284.6 eV of adventitious carbon. The peak of O1s region was analyzed by XPSPEAK software (version 4.0).

Electrolytes and Catalysts Preparation

Preparation of carbonate buffer solutions

The CO₂/HCO₃⁻ solution (pH = 6.90) was acquired by vigorously bubbling CO₂ to a 0.2 M NaHCO₃ aqueous solution for at least 30 min. The HCO₃⁻/CO₃²⁻ solution (pH = 9.20) was prepared by slowly adding NaOH to a 0.2 M NaHCO₃ solution. The pH value was monitored by pH meter (Mettler Corp.). The HCO₃⁻/CO₃²⁻ solution (pH = 9.75) was obtained by mixing equal volume of 0.2 M NaHCO₃ and 0.2 M Na₂CO₃ aqueous solutions.

Iron-carbonate (Fe-Ci) Catalysts Preparation

Synthesis of the catalyst was carried out in an undivided gas-tight three-electrode configuration by using a CHI 630E Electrochemical Analyzer (Shanghai Chenhua Instrument Co., LTD). A piece of FTO glass slide, washed with acetone, ethanol, and

then de-ionized water, was put into the above solution as the working electrode. The area of FTO immersed in solution was 1 cm². Ag/AgCl (4M KCl) and Pt wire were used as the reference electrode and the counter electrode, respectively. The reference electrode was calibrated by using redox couple [Ru(bpy)₃]³⁺/[Ru(bpy)₃]²⁺ ($E_{1/2} = 1.26$ V vs. NHE) as a standard. Prior to dissolution of iron (II) sulfate, a 0.2 M NaHCO₃ solution was vigorously bubbled with CO₂ for at least 30 min. Then FeSO₄·7H₂O (1 mM) was added to the CO₂ saturated NaHCO₃ solution (pH = 6.90). A constant potential of 1.37 V vs. NHE was applied and the electrodeposition was carried out in quiescent solution. The deposition time was dependent on the required passed charge. The passed charge was 30 mC/cm² for long-term electrolysis and 10 mC/cm² for other electrochemical experiments. A typical i-t plot of deposition was showed in Figure S2. The resulting film was washed with de-ionized water after deposition. Before electrochemical measurement, the as-prepared film was put into a 0.2 M NaHCO₃/Na₂CO₃ solution (pH = 9.75) for anodization at 1.20 V vs. NHE for *ca.* 2 h (Figure S3).

The iron coverage of deposited film was ascertained by the ICP-AES (Inductively Coupled Plasma-Atomic Emission). A 1 cm² sample was dissolved in 5.0 mL of 2 M HNO₃ for measurement. The iron concentration of 1.019 mg/L was obtained using the working curve method, which suggested that 91.2 nmol of iron was electrodeposited onto 1.0 cm² of FTO electrode. The calculated passing charge of 8.80 mC/cm² agreed well with measured charge (10 mC/cm²).

Electrochemical measurements

All electrochemical measurements were carried out at room temperature (298±1 K) by using a CHI 630E Electrochemical Analyzer (Shanghai Chenhua Instrument Co., LTD). An undivided three-electrode configuration with 25 mL electrolyte was used in all the experiments. A 1 cm² FTO with or without modified catalysts was the working electrode. Ag/AgCl (4 M KCl) was used as the reference electrode, and Pt wire was the counter electrode. All potentials in following experiments were reported

versus the normal hydrogen electrode (NHE), and the reference electrode was calibrated by redox couple $[\text{Ru}(\text{bpy})_3]^{3+}/[\text{Ru}(\text{bpy})_3]^{2+}$ ($E_{1/2} = 1.26 \text{ V vs. NHE}$) as a standard. All the Cyclic voltammograms (CVs) were carried out in quiescent solutions with a scan rate as 50 mV/s. Constant potential electrolysis (CPE) was carried out at 1.20 or 1.30 V with gently stirring (500 r/min). When necessary, the resistance was corrected by automatic iR compensation function available on the CHI potentiostats.

Tafel plot Measurements

Current-potential data were acquired by implementing controlled potential electrolysis in 25 mL of 0.2 M pH = 9.75 $\text{HCO}_3^-/\text{CO}_3^{2-}$ buffer solution at a variety of applied potentials. The working electrode was 1 cm² FTO electrode fabricated with Fe-Ci films (after anodization). Ag/AgCl (4M KCl) and Pt wire were used as the reference electrode and the counter electrode, respectively. All data were collected with iR compensation (the measured resistance of the solution was *ca.* 30 Ω). The stable currents were recorded at applied potentials ranging from 1.06 to 1.15 V in every 10 mV step for 300 s CPE experiments with gently stirring. Typically, the current densities were ranging from 3.44 $\mu\text{A}/\text{cm}^2$ to 1.23 mA/cm^2 .

Current-pH plot measurements

The data were collected by implementing controlled potential electrolysis in 25 mL of 0.2 M carbonate buffer solution at a variety of pH values and a constant applied bias of 1.10 V. The solution pH was adjusted by slowly adding NaOH. The working electrode was 1 cm² FTO electrode fabricated with Fe-Ci films (after anodization). Ag/AgCl (4M KCl) and Pt wire were used as the reference electrode and the counter electrode, respectively. All data were collected with iR compensation. The pH values of carbonate buffer solution were ranging from 9.5 to 10.1 with 0.1 pH step for 300 s CPE experiments with gently stirring. The measured current densities ranging from 13.4 $\mu\text{A}/\text{cm}^2$ to 0.158 mA/cm^2 were among the linear region of Tafel plot.

Current-buffer concentration plot measurements

The results were collected by implementing CPE in 25 mL carbonate buffer solution at a variety of electrolyte concentration while the constant applied bias was 1.08 V, 1.10 V and 1.12 V. The overall concentrations were maintained as 0.5 M by adding NaClO₄. The working electrode was 1 cm² FTO electrode fabricated with Fe-Ci films (after anodization). Ag/AgCl (4M KCl) and Pt wire were used as the reference electrode and the counter electrode, respectively. All data were collected with iR compensation. The concentrations of carbonate buffer solution were ranging from 0.002 to 0.2 M for 300 s CPE experiments with gently stirring. The steady current density was among the linear region in Tafel plot, which was typically ranging from 4.4 μA/cm² to 121.2 μA/cm².

Determination of Faradaic efficiency

The experimental setup was a home-made single compartment gas-tight cell equipped with Fe-Ci coated FTO (0.7 cm² immersed area) as the working electrode, Ag/AgCl (4 M KCl) as the reference electrode and Pt mesh as the counter electrode. Prior to measurement, the solution was degassed by bubbling Ar for 1 h. The experiment was carried out at 1.30 V without iR compensation in 0.2 M pH 9.75 Fe²⁺-free carbonate buffer solution for 6 h. During the bulk electrolysis, the amount of evolved oxygen in the headspace was quantified by gas chromatography (Figure S8).

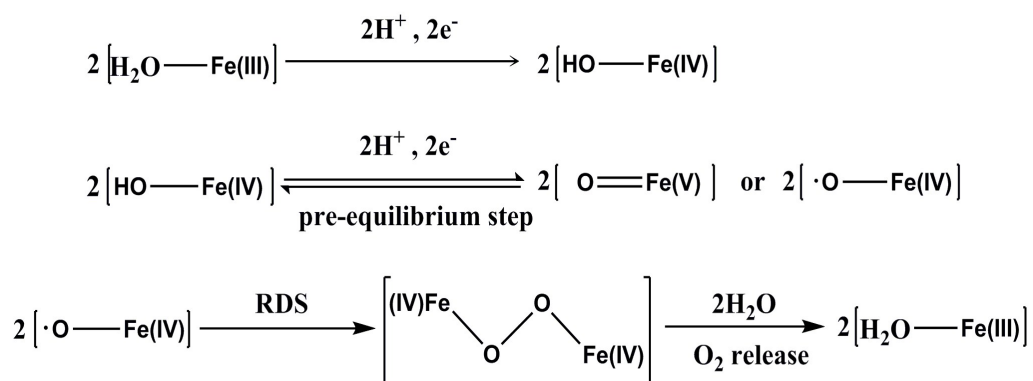
Possible Reaction Mechanism

According to previous studies on cobalt and nickel oxides, the electrochemical kinetics of electrode surface could be depicted as a mechanistic sequence involving a reversible n_1 proton and n_2 electron pre-equilibrium step followed by a rate-limiting chemical step (eq. S1-S2).^{1,2}





Based on the electrochemical kinetics analysis in this study (see main text), a possible reaction mechanism of Fe-Ci was deduced as Scheme S1. In light of the main valence state of three for iron atoms, the active site was proposed to consist of two adjacent [Fe(III)-OH₂] motifs, which are subjected to rapid oxidation process to form [Fe(IV)-OH]. The subsequent 2e⁻/2H⁺ quasi-equilibrium step may be related to the generation of [Fe(V)=O] or [Fe(IV)-O·]. This step is followed by O-O bond formation through a radical coupling of two adjacent [Fe(IV)-O·] species, which is the RDS of the whole catalytic cycle. Finally, [Fe(III)-OH₂] is regenerated by oxygen release and water coordination. It should be noted that [Fe(III)-OH₂], [Fe(IV)-OH], and [Fe(IV)-O·] do not represent the genuine species on the electrode surface because protons and holes might be delocalized in possible adjacent bridging O atoms.¹⁻³ Future research on the key intermediates is definitely required to testify and consummate this hypothetical mechanism.



Scheme S1. Proposed pathway for oxygen evolution by Fe-Ci in pH 9.75 HCO₃⁻/CO₃²⁻ buffer.

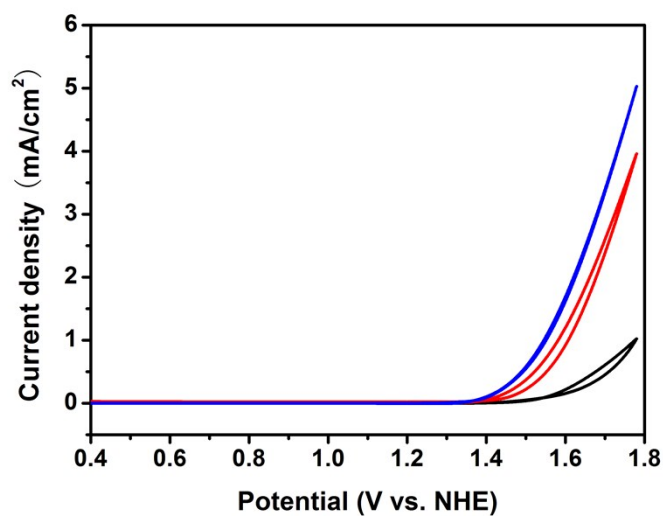


Figure S1 CVs of FTO electrode in 0.2 M CO₂ saturated NaHCO₃ electrolyte (pH = 6.90) with (red) and without (black) the presence of 1 mM Fe²⁺. CV of Fe-Ci modified FTO electrode in a Fe²⁺ free CO₂ saturated NaHCO₃ electrolyte (pH = 6.90) is shown as blue solid curve. No iR compensation was applied.

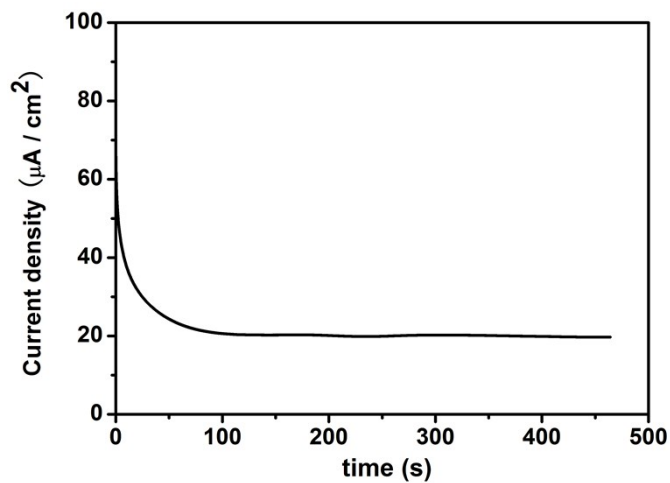


Figure S2 Representative curve of deposition of FTO electrodes in 0.2 M CO₂ saturated NaHCO₃ solution (pH = 6.9) contained 1 mM FeSO₄. RE: Ag/AgCl; CE: Pt wire; applied potential: 1.37 V.

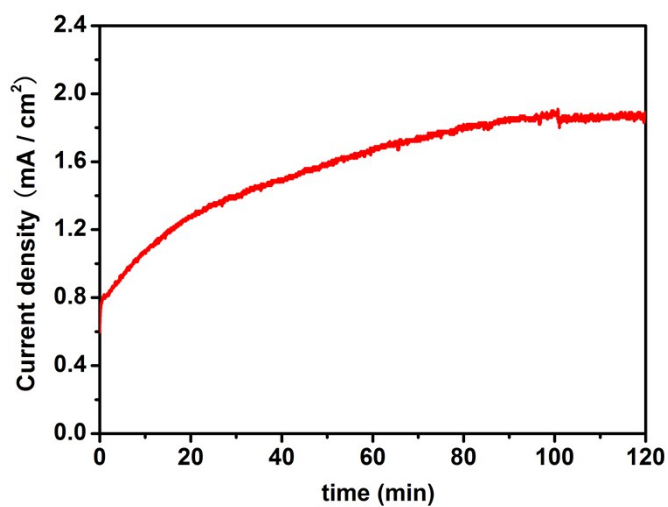


Figure S3 Representative curve of anodization of freshly deposited Fe-Ci electrode in Fe²⁺ free HCO₃⁻/CO₃²⁻ solution (0.2 M, pH 9.75). RE: Ag/AgCl; CE: Pt wire; applied potential: 1.20 V; electrode area: 1 cm². No iR compensation was applied.

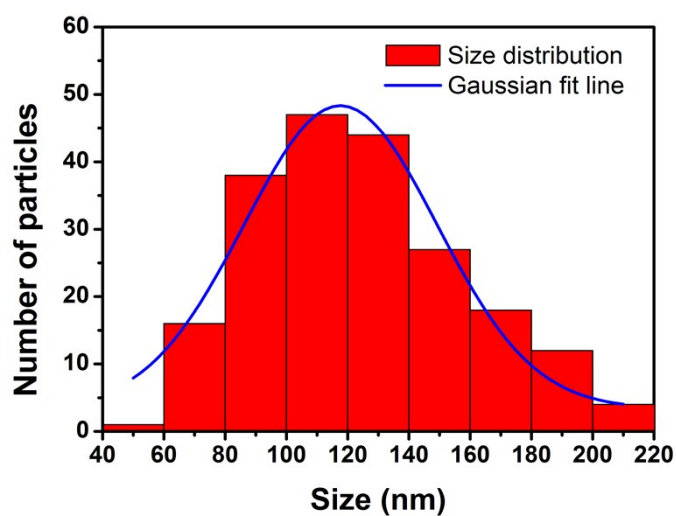


Figure S4 Size distribution histogram (red) of the Fe-Ci particles based on Figure 2b. The blue curve is the Gaussian fit line.

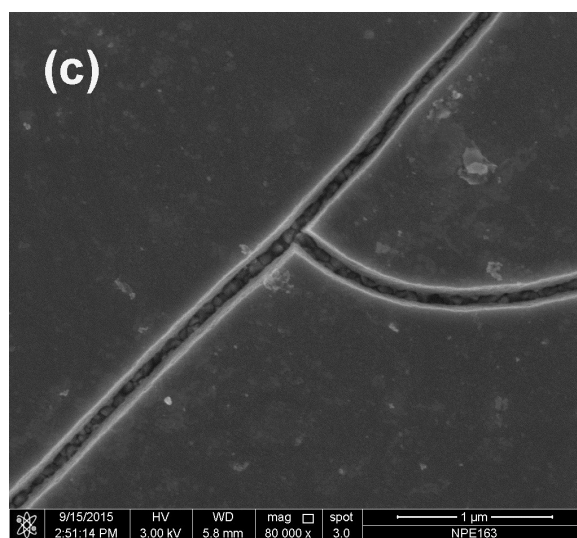
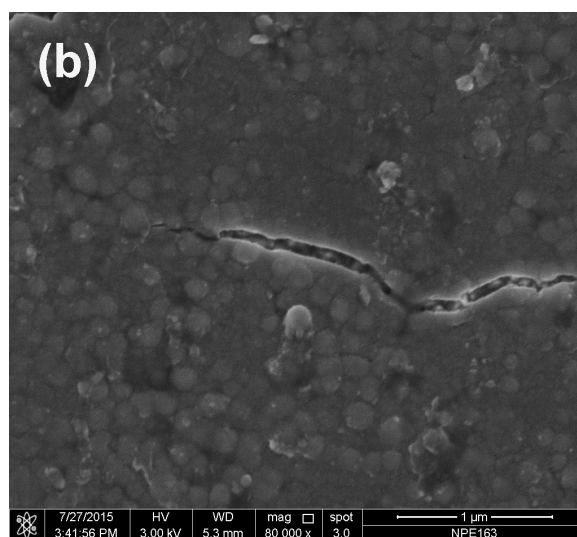
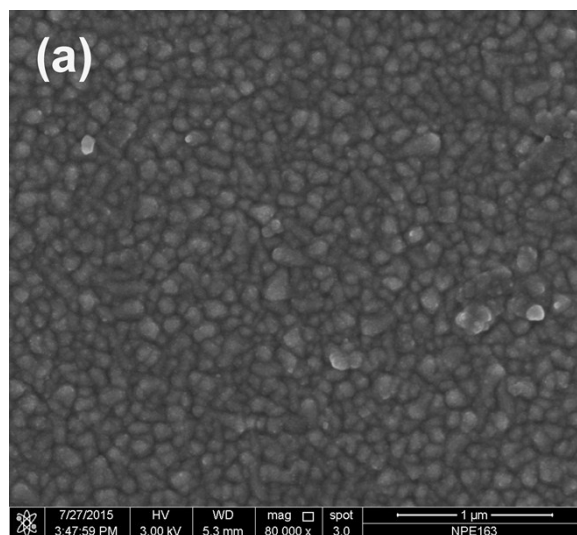


Figure S5 SEM images of the Fe-Ci modified FTO electrodes. The charges passed during electrodeposition are (a) 10 mC/cm²; (b) 60 mC/cm² and (c) 120 mC/cm², respectively.

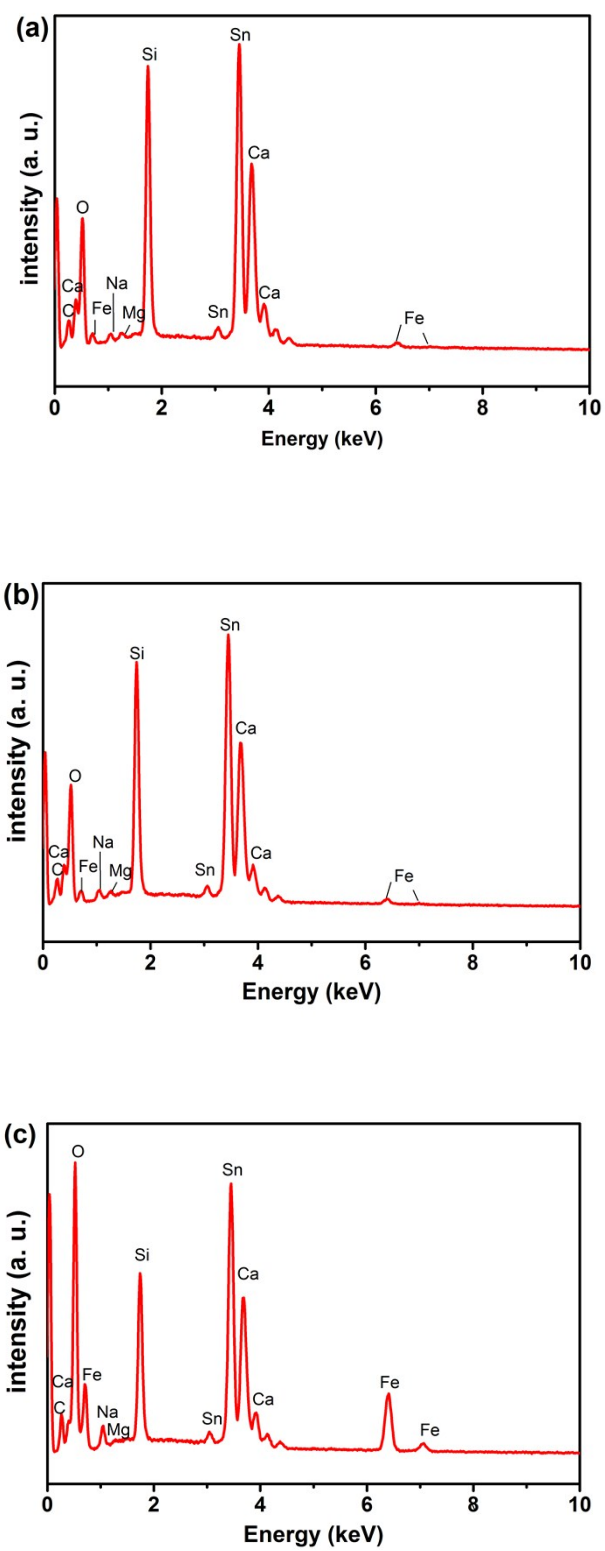


Figure S6 EDX spectra of the Fe-Ci modified FTO electrode. The charges passed during electrodeposition are (a) 10 mC/cm²; (b) 60 mC/cm² and (c) 120 mC/cm², respectively.

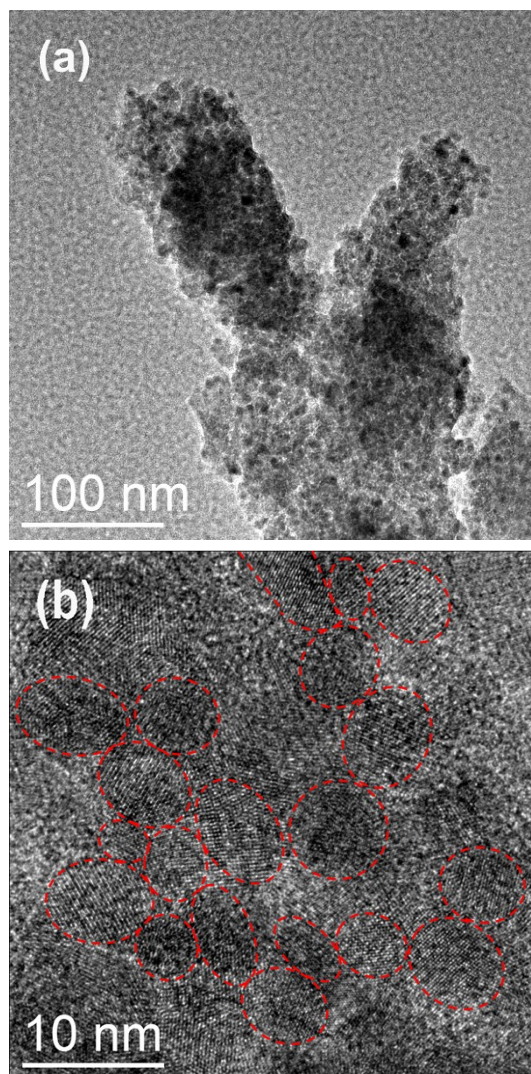


Figure S7 (a) TEM and (b) HRTEM images of the Fe-Ci catalyst scrapped from FTO electrode (10 mC/cm²). The red dashed circles indicate the interconnected tiny particles.

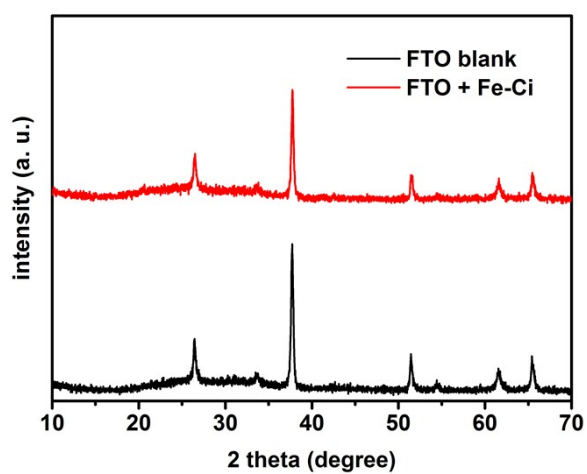


Figure S8 PXRD pattern of the FTO electrodes with (red) and without (black) Fe-Ci modification.

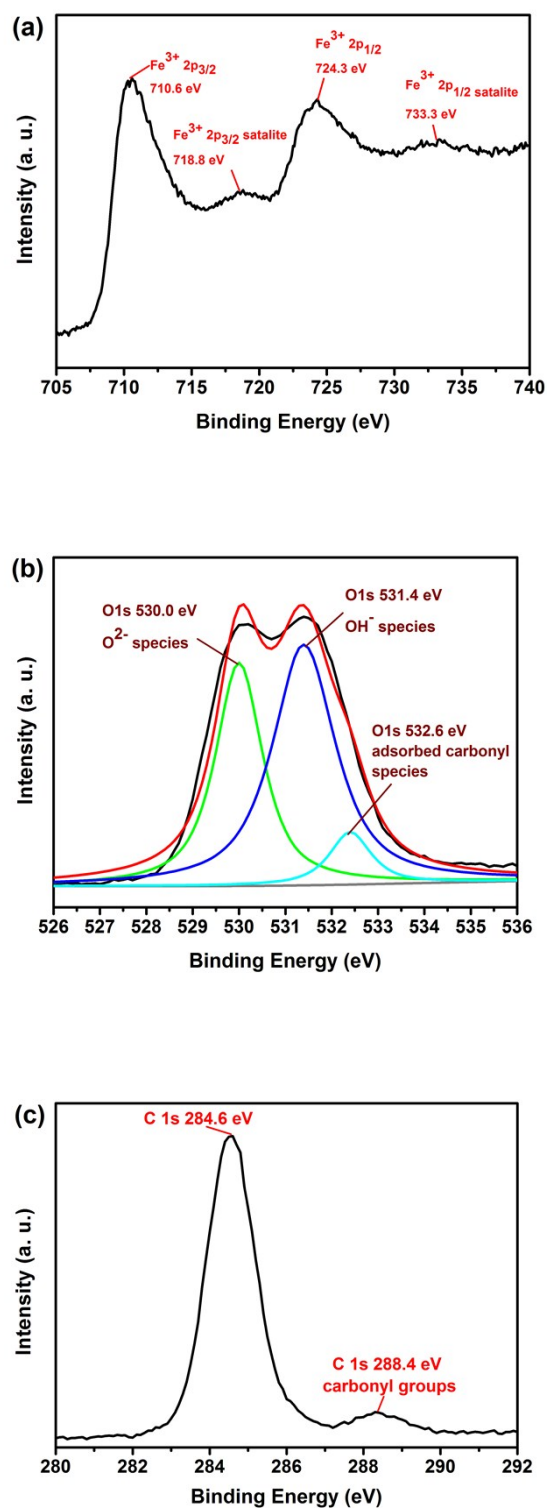


Figure S9 Sections of the XPS spectrum around the Fe 2p (a), O 1s (b) and C 1s (c) energy regions. For Figure S9b, the black and the red curves represent the original and the optimized curves, respectively. The XPS spectrum of the O 1s energy region can be resolved with three subpeaks attribute to O²⁻ (green), OH⁻ (blue) and carbonyl group (cyan), respectively. The background is shown in gray.

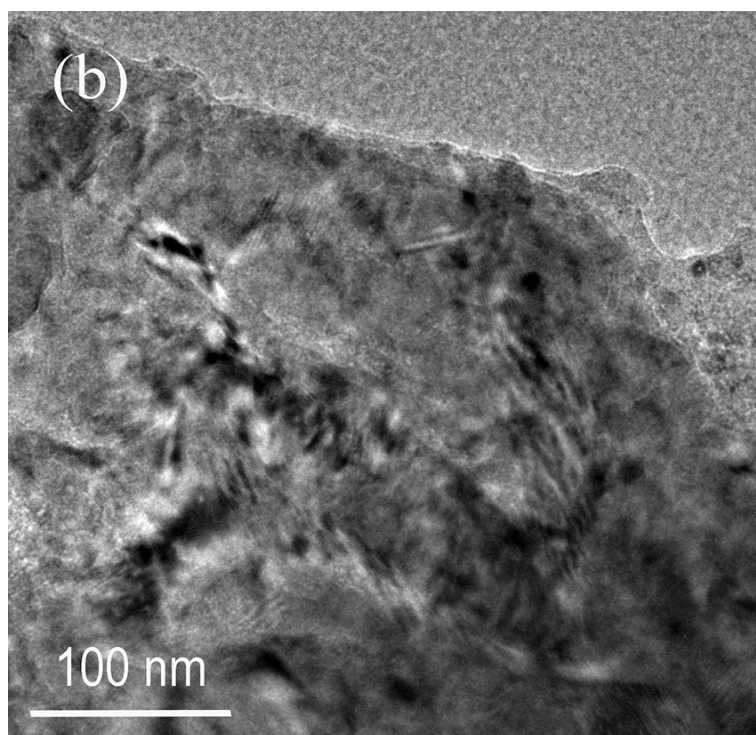
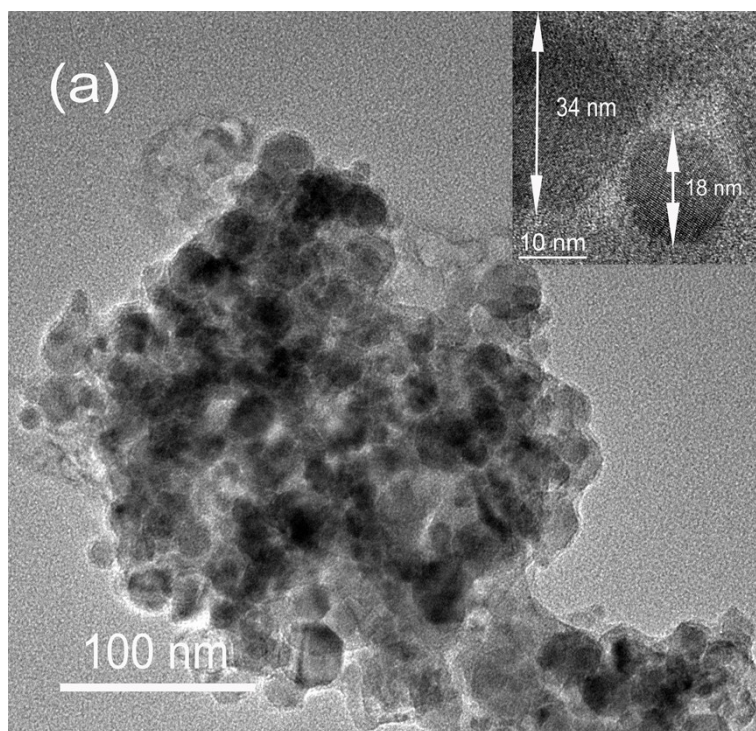


Figure S10 TEM images of the Fe-Ci catalyst scrapped from FTO electrode. The charges passed during deposition are (a) 60 mC/cm² and (b) 120 mC/cm², respectively. The inset of (a) is the HRTEM image of the aggregated particles.

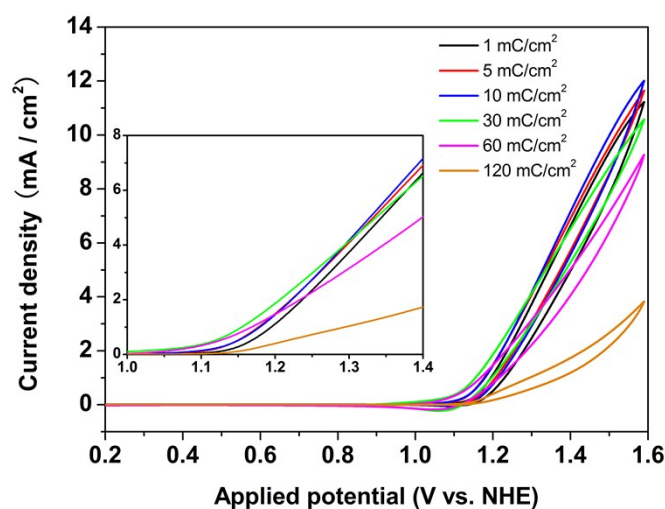


Figure S11 CVs of Fe-Ci modified FTO electrodes with different amounts of charges passed during deposition. Inset shows the enlarged anodic polarization curves for clarity. Electrolyte: 0.2 M $\text{HCO}_3^-/\text{CO}_3^{2-}$ solution (0.2 M, pH 9.75); RE: Ag/AgCl; CE: Pt wire; scan rate: 50 mV/s; electrode area: $A = 1 \text{ cm}^2$. No iR compensation was applied.

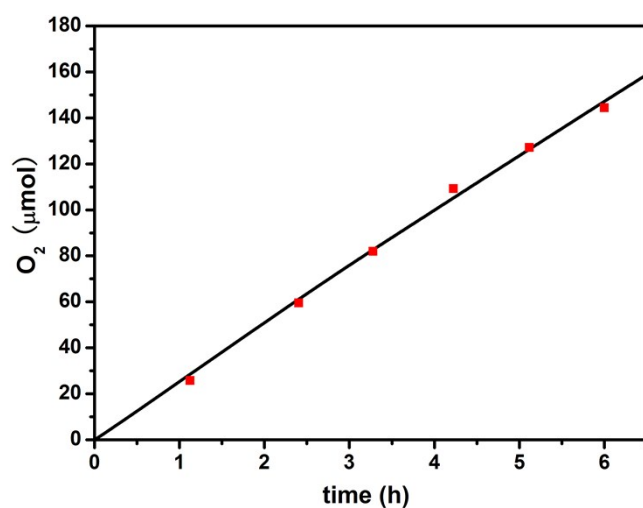


Figure S12 Determination of Faradaic efficiency. Line: Theoretical amount of oxygen as assumed by passed charge with 100% Faradaic efficiency. Square: The amount of generated oxygen measured by gas chromatography. Electrolyte: 0.2 M pH 9.75 $\text{HCO}_3^-/\text{CO}_3^{2-}$ solution; applied bias: 1.30 V (no iR compensation); WE: 0.7 cm^2 Fe-Ci modified FTO; RE: Ag/AgCl; CE: Pt mesh.

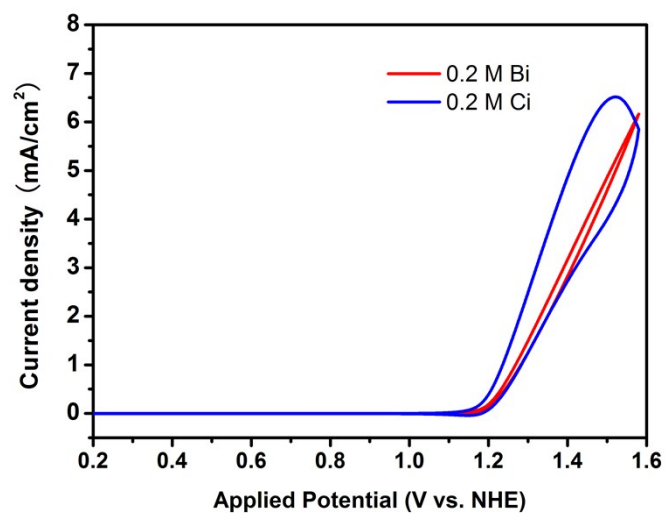


Figure S13 CVs of Fe-Ci catalyst modified FTO electrode in 0.2 M pH 9.2 borate (red) and carbonate (blue) buffer solutions. RE: Ag/AgCl; CE: Pt wire; scan rate: 50 mV/s; electrode area: $A = 1 \text{ cm}^2$. No iR compensation was applied.

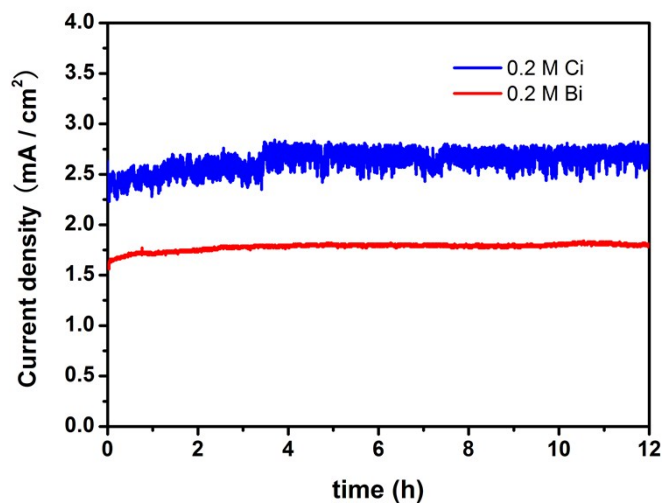


Figure S14 Constant potential electrolysis of catalyst-coated FTO in Fe^{2+} free 0.2 M pH 9.2 borate (red) and carbonate (blue) buffer solutions with gently stirring at a potential of 1.30 V (no iR compensation). RE: Ag/AgCl; CE: Pt wire; electrode area: $A = 1 \text{ cm}^2$.

Table S1 Comparison of catalytic performances and working conditions for a variety of WOCs containing earth-abundant transition metals. The overpotential (η) is determined from the Tafel plots because the CVs were not resistance corrected in some reports.

Cat.	η at 0.01 mA/cm ² (V)	η at 1 mA/cm ² (V)	Tafel Slope (mV / decade)	Electrolyte (pH)	Reference
Co-Pi	0.28	0.41	60	0.1 M Pi (7.0)	[4]
Co-Bi	0.28	0.40	60	0.1 M Bi (9.2)	[5]
Co-W	0.21 ^a	0.34 ^b	133	0.05 M Na ₂ WO ₄ (8.0)	[6]
Ni-Bi	0.31	0.42	58	0.2 M Bi (9.2)	[7]
Ni-Gly	0.43 ^a	0.48	40	0.25 M Pi (11.0)	[8]
Cu-Ci	0.38 ^c	0.48	90	1 M Na ₂ CO ₃ (10.8)	[9]
Cu-Bi	0.35	0.53	89	0.2 M Bi (9.0)	[10]
Cu-tpa	0.43	0.60	56	0.1 M Bi (9.2)	[11]
MnOx	0.43	0.58	76	0.1 M Pi (7.0)	[12]
Sub-MnOx	0.35 ^c	0.42	73	0.3 M Pi (7.8)	[13]
Fe-Ac	0.42	0.52	52	0.1 M Pi (7.0)	[14]
Fe-HEPES	0.44	0.49 ^c	47	0.1 M Pi (7.0)	[15]
a-FeOx	0.32	0.41	40	0.1 M KOH (13.0)	[16]
a-FeNiOx	0.21	0.26	24	0.1 M KOH (13.0)	[16]
Fe-Ci	0.43	0.50^d	34	0.2 M Ci (9.75)	This work

a. overpotential at 0.05 mA/cm²

b. overpotential at 0.5 mA/cm²

c. overpotential at 0.1 mA/cm²

d. The current density is 1.23 mA/cm² at $\eta = 0.50$ V

References

1. Y. Surendranath, M. W. Kanan and D. G. Nocera, *J. Am. Chem. Soc.*, 2010, **132**, 16501.
2. D. K. Bediako, Y. Surendranath and D. G. Nocera, *J. Am. Chem. Soc.*, 2013, **135**, 3662.
3. G. L. Elizarova, L. G. Matvienko, V. L. Kuznetso, D. I. Kochubey and V. N. Parmon, *J. Mol. Catal. A*, 1995, **103**, 43.
4. M. W. Kanan and D. G. Nocera, *Science*, 2008, **321**, 1072.
5. Y. Surendranath, M. Dincă and D. G. Nocera, *J. Am. Chem. Soc.*, 2009, **131**, 2615.
6. B. Zhang, X. Wu, F. Li, F. Yu, Y. Wang and L. Sun, *Chem. Asian J.*, 2015, **10**, 2228.
7. M. Dincă, Y. Surendranath, D. G. Nocera, *Proc. Natl. Acad. Sci. USA* 2010, **107**, 10337.
8. D. Wang, G. Ghirlanda and J. P. Allen, *J. Am. Chem. Soc.*, 2014, **136**, 10198.
9. J. Du, Z. Chen, S. Ye, B. J. Wiley and T. J. Meyer, *Angew. Chem. Int. Ed.*, 2015, **54**, 2073.
10. F. Yu, F. Li, B. Zhang, H. Li and L. Sun, *ACS Catal.*, 2015, **5**, 627.
11. X. Liu, H. Jia, Z. Sun, H. Chen, P. Xu and P. Du, *Electrochem. Commun.*, 2014, **46**, 1.
12. I. Zaharieva, P. Chernev, M. Risch, K. Klingan, M. Kohlhoff, A. Fischer and H. Dau, *Energy Environ. Sci.*, 2012, **5**, 7081.
13. K. Jin, A. Chu, J. Park, D. Jeong, S. E. Jerng, U. Sim, H. Y. Jeong, C. W. Lee, Y. S. Park, K.

- D. Yang, G. K. Pradhan, D. Kim, N. E. Sung, S. H. Kim and K. T. Nam, *Sci. Rep.*, 2015, **5**, 10279.
14. Y. Wu, M. Chen, Y. Han, H. Luo, X. Su, M. T. Zhang, X. Lin, J. Sun, L. Wang, L. Deng, W. Zhang and R. Cao, *Angew. Chem. Int. Ed.*, 2015, **54**, 4870.
15. M. Chen, Y. Wu, Y. Han, X. Lin, J. Sun, W. Zhang and R. Cao, *ACS Appl. Mater. Interfaces*, 2015, **7**, 21852.
16. R. D. Smith, M. S. Prevot, R. D. Fagan, Z. Zhang, P. A. Sedach, M. K. Siu, S. Trudel and C. P. Berlinguette, *Science*, 2013, **340**, 60.